Journal of Power Sources 241 (2013) 168–172

Contents lists available at SciVerse ScienceDirect

Journal of Power Sources

journal homepage: www.elsevier.com/locate/jpowsour

Short communication

A composite film of reduced graphene oxide modified vanadium oxide nanoribbons as a free standing cathode material for rechargeable lithium batteries

Yi Sun [a,b], Shu-Bin Yang [b], Li-Ping Lv [b], Ingo Lieberwirth [b], Lin-Chao Zhang [a], Chu-Xiong Ding [a], Chun-Hua Chen [a,*]

[a] CAS Key Laboratory of Materials for Energy Conversion, Department of Materials Science and Engineering, University of Science and Technology of China, Hefei, Anhui 230026, China
[b] Max Planck Institute for Polymer Research, Mainz 55128, Germany

HIGHLIGHTS

- RGO modified hydrated vanadium pentoxide nanoribbons are obtained by a facile hydrothermal process.
- A free-standing $VO_{2.07}$/RGO film is fabricated with these ribbons.
- The binder-free free-standing $VO_{2.07}$/RGO film electrode shows good electrochemical properties.

ARTICLE INFO

Article history:
Received 7 February 2013
Received in revised form
19 April 2013
Accepted 20 April 2013
Available online 29 April 2013

Keywords:
Vanadium oxide
Graphene
Nanoribbon
Cathode
Lithium battery

ABSTRACT

Hydrated vanadium pentoxide ($V_2O_5 \cdot 0.86H_2O$) nanoribbons modified with reduced graphene oxide (RGO) are synthesized by a hydrothermal process. These ribbons are 30 nm thick, 200 nm to 1 μm wide and above 50 μm long. Binder-free films are prepared by using these ribbons and annealed at 300 °C in nitrogen as the cathode for rechargeable lithium cells. The intertwining network of this free-standing VO_x/RGO film provides efficient conduction pathways for electrons and short diffusion distances for Li ions. The electrochemical tests exhibit that this cathode film delivers a high reversible specific capacity (160 mAh g^{-1}) and good cycling stability (133 mAh g^{-1} after 200 cycles) in the voltage range between 2.0 and 3.5 V.

1. Introduction

Nowadays, the portable electronic devices have been widely used in our daily life. Nevertheless, in order to meet the needs of various new specifications, e.g. paper thin, lightweight and low cost, the power sources of these devices, such as rechargeable Li-ion batteries, are desired to further improve the power and energy density, safety and cycling stability. For traditional Li-ion battery electrodes, polymer binders are added to bind active materials to current collectors, which are mainly copper (10 mg cm^{-2}) or aluminum (5 mg cm^{-2}) foil. This causes an undesirable decrease of electrical conductivity and energy density. Recently, free-standing electrodes have been prepared by carbon based nanomaterials, such as carbon nanotubes [1,2] or graphene sheets [3,4], and silicon particles [5] or metal oxides [6] can be incorporated as active materials.

Vanadium oxides with multiple valence states from +2 in VO to +5 in V_2O_5 have been extensively studied for the potential applications in lithium ion batteries due to the low cost and high energy density [7–10]. V_2O_5 is known for various phase transformations during Li^+ intercalation/deintercalation process that deliver high theoretical capacities up to 294 ($x = 2$ in $Li_xV_2O_5$) and 442 mAh g^{-1} ($x = 3$ in $Li_xV_2O_5$). Moreover, it was reported that V_2O_5 xerogels and aerogels can react with 4 Li and 5.8 Li per mole of V_2O_5, respectively, corresponding to capacities of 560 and 650 mAh g^{-1}, which are much higher than those of $LiCoO_2$ and $LiFePO_4$ cathodes [11,12]. However, it suffers from a large irreversible capacity loss at deep charge/discharge depth ($x > 1$ in $Li_xV_2O_5$), resulting in fast capacity fading [13,14]. In addition to V_2O_5, VO_2 is

* Corresponding author. Tel.: +86 551 63606971; fax: +86 551 63601592.
E-mail address: cchchen@ustc.edu.cn (C.-H. Chen).

0378-7753/$ – see front matter © 2013 Elsevier B.V. All rights reserved.
http://dx.doi.org/10.1016/j.jpowsour.2013.04.093

found to show a better cycling stability with a theoretical capacity of 161 mAh g^{-1} (corresponding to 0.5 lithium insertion/extraction per unit formula). To develop high-performance VO_2 based cathodes, one-dimensional (1D) nanowires or nanoribbons are the most favorable as they can offer large interfacial contact area between the electrode and electrolyte, efficient 1D electron transport pathways, limited volume change and short lithium transport distance [15–17].

Recently, graphene has been widely investigated as an important component in the composites for vanadium oxide-based electrode materials [18–21]. Here, we report that hydrated vanadium pentoxide nanoribbons modified with reduced graphene oxide (RGO) are fabricated by a hydrothermal approach. These ribbons are further used to prepare a free-standing film without addition of any binders, then annealed at 300 °C in nitrogen to obtain $VO_{2.06}$/RGO film electrode. The intertwining network structure provides efficient electron conduction pathways and short Li^+ diffusion distances. The electrochemical tests reveal that the free-standing film cathode delivers a high reversible specific capacity (160 mAh g^{-1}) and good cycling stabilities (133 mAh g^{-1} after 200 cycles) in the voltage range of 2.0–3.5 V.

2. Experimental section

The graphene oxide was synthesized from natural flake graphite by a modified Hummers method [22], the details of which were described elsewhere [23]. In the hydrothermal process, 3 mg graphene oxide was firstly dispersed in 10 ml aqueous solution containing 50 mg cetyl trimethylammonium bromide (CTAB), and then ultrasonically treated for 1 h. After stirring for 10 min, 2 ml of 0.1 M NH_4VO_3 in 1 M HNO_3 aqueous solution was added. Then the mixture was transferred to a Teflon-lined stainless steel autoclave (20 ml in volume) and kept in an electric oven at 180 °C for 20 h. The product was collected by centrifugation and washing with warm ethanol for several times.

To fabricate the free-standing electrode, the obtained product was dispersed in an ethanol solution under ultrasonication for 5 min. The mixture was poured into a funnel with a filtration membrane at the bottom and dried in an oven at 60 °C under normal pressure. After the evaporation of ethanol, a free-standing film was easily peeled off from the membrane. Then some free-standing electrodes were made by punching the film into small disks (10 mm in diameter) and annealing at 300 °C in nitrogen for 2 h. For comparison, a free-standing vanadium oxide electrode was also fabricated by the same procedure but without adding graphene oxide in the hydrothermal step.

The samples were analyzed with an X-ray diffractometer in a 2θ range between 10 and 60° (Rigaku TTR-III, Cu Kα radiation). Their morphologies were analyzed under a scanning electron microscope (SEM, LEO 1530) and a transmission electron microscope (TEM, FEI Tecnai F20). The thermogravimetric analysis (TGA) was conducted with a thermogravimetry analyzer (Shimadzu, TGA-50) under ambient atmosphere with a heating rate of 5 °C min^{-1} from room temperature to 700 °C. X-ray photoelectron spectroscopy (XPS) measurement was performed on VG Scienta-R3000 using an Al Kα sources 1846.6 eV anode. All the binding energies were calibrated to C1s peak at 284.3 eV of carbon.

The electrochemical properties of these free-standing electrodes were measured using CR2032 coin type cells with the films as the working electrodes, Li as the counter electrode, and 1 M $LiPF_6$ in ethylene carbonate and diethyl carbonate (EC:DEC = 1:1 v/v) as the electrolyte. The mass loading of the film electrode is 1.2 mg cm^{-2}. The cells were assembled in an argon-filled glove box (MBraun Labmaster 130) containing less than 1 ppm each of moisture and oxygen. The discharge and charge measurements were carried out in the voltage range between 2.0 and 3.5 V on a battery test system (Neware BTS-610). The electrochemical impedance spectra (frequency range: 0.001–10^5 Hz) were measured on an electrochemical workstation (CHI 660C).

3. Results and discussions

The XRD pattern of the $VO_x \cdot xH_2O$/RGO sample obtained after the hydrothermal treatment is shown in Fig. 1a. It displays a set of characteristic (00*l*) peaks for a layered phase $V_2O_5 \cdot xH_2O$, which is in a good agreement with the standard pattern (JCPDS card No.40-1296). An additional diffraction shoulder peak at 2θ = 25.5°, partially overlapping with the $V_2O_5 \cdot xH_2O$ (003) peak, originates from the (002) peak of disorderedly stacked RGO sheets in the sample [24,25]. The layer spacing of the phase is calculated to be 11.5 Å from 001 reflection, which is well above the (00*l*) spacing of layered V_2O_5 due to the presence of H_2O molecules embedded between the layers of basic VO_5 pyramid units. According to Giorgetti et al. [26] and Liu et al. [27], these ribbons could be with a possible bilayer structure. According to the TGA data of the sample without RGO (Fig. 1b, curve i), the weight losses of about 1.2% below 100 °C and about 7.8% in the temperature range of 200–450 °C are attributed to the evaporation of adsorbed water and the removal of coordinated water, respectively. Thus, the x in $V_2O_5 \cdot xH_2O$ is determined to be 0.86. As shown in SEM images (Fig. 2a and b), a large number of ribbons with a thickness of about 30 nm, a width from 200 nm to 1 μm and a length above 50 μm can be observed. The top-down view of the film does not clearly show any RGO due to the penetration of electrons through the thin sheets, but some sheets can still be distinguished because they are wrinkled (Fig. 2b). Some of the ribbons are grown together in the form of bundles, which exhibit larger size in width (inset of Fig. 2b). TEM images show the RGO sheets wrinkle at the edge of the ribbons and cover

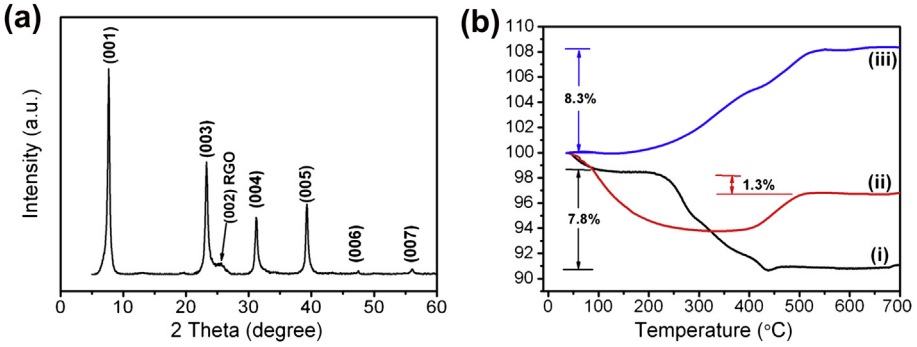

Fig. 1. (a) XRD pattern of the $V_2O_5 \cdot xH_2O$/RGO ribbons after hydrothermal process; (b) TGA curves of (i) $V_2O_5 \cdot xH_2O$ ribbons without RGO, (ii) the ribbons with RGO after annealing, (iii) the ribbons without RGO after annealing.

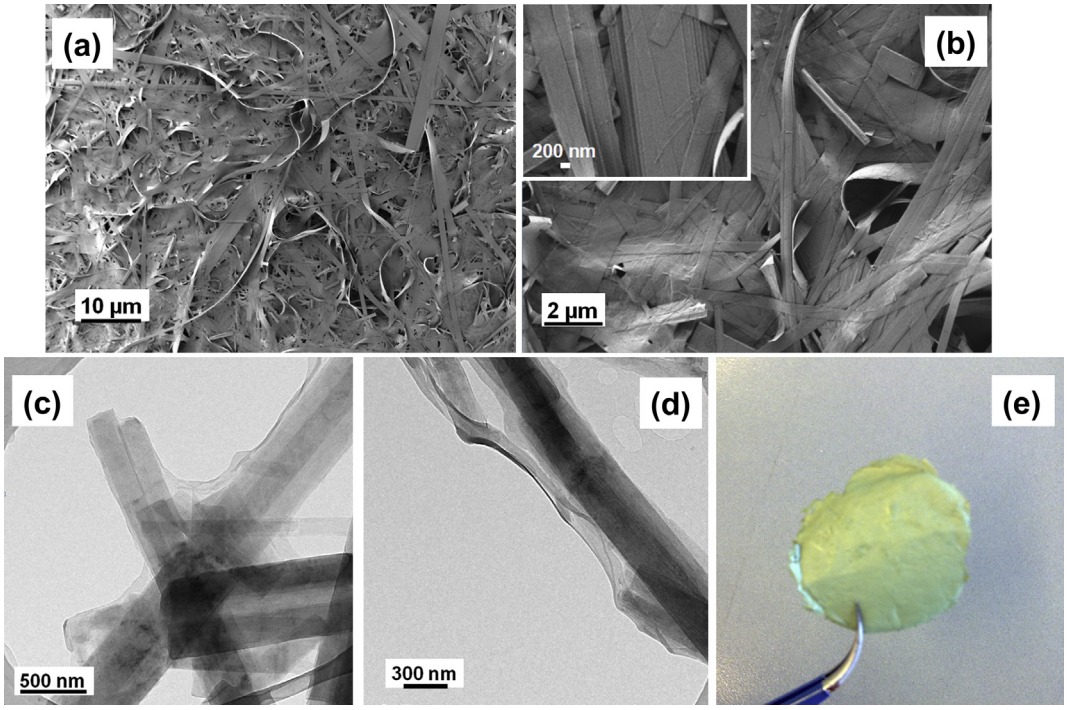

Fig. 2. (a, b) SEM and (c, d) TEM images of the $V_2O_5{\cdot}xH_2O$/RGO ribbons composite; (e) optical image of free-standing $V_2O_5{\cdot}xH_2O$/RGO film on the intertwining network of above ribbons without addition of any binders.

on their surface (Fig. 2c and d). Based on these RGO-modified hydrated vanadium pentoxide ribbons, the free-standing film is facilely fabricated with an intertwining network (Fig. 2e).

In order to achieve better electrochemical performance, the as-prepared free-standing film was then annealed at a relatively low temperature of 300 °C in nitrogen to obtain a dehydrated VO_x/RGO film electrode. The XRD pattern of the annealed film is shown in Fig. 3a. The film can be identified as VO_2 (JCPDS card No.81-2393) of poor crystallinity, meaning V^{5+} is reduced to V^{4+} during the annealing process. To further confirm the oxidation state of vanadium, X-ray photoelectron spectroscopy analysis is also carried out. Compared to that of a pure V_2O_5, the spectrum of the sample shifts

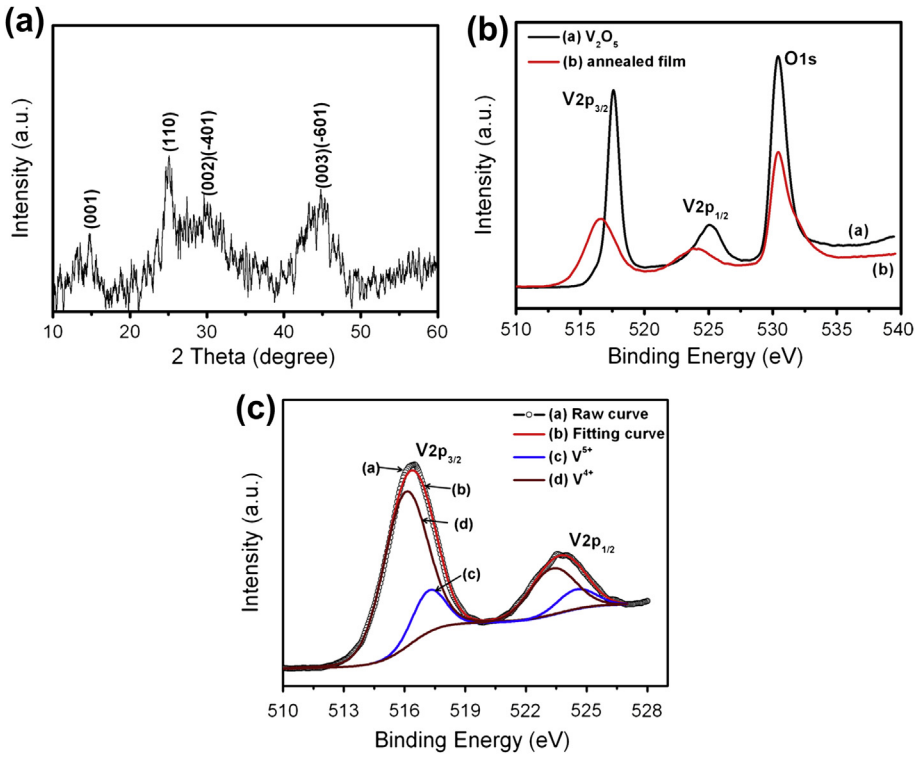

Fig. 3. (a) XRD pattern of the VO_x/RGO film electrode; (b) XPS spectrum for the O 1s and V 2p bands of the VO_x/RGO film and V_2O_5; (c) fitting-curves of V_{2p} peaks of VO_x/RGO film.

to lower binding energy, indicating the reduction state of vanadium (Fig. 3b). The V 2p spectrum of the film is observed with the binding energy at around 516.4 eV (V $2p_{3/2}$) and 523.8 eV (V $2p_{1/2}$), indicating the existences of both V^{5+} and V^{4+}. In order to estimate the contents of each valence state of vanadium, the spectrum can be fitted well by the summation of four spectra: the peaks at 517.2 and 524.5 eV corresponding to V^{5+}; the peaks at 516 and 523.3 eV corresponding to V^{4+} (Fig. 3c). These assignments are in good agreement with the literature values [28,29]. The TGA curve of the annealed film without RGO (Fig. 1b, curve iii) shows a weight increase of about 8.3% in the temperature range of 200–500 °C, which is less than the calculated weight increase (9.6%) from pure VO_2 to pure V_2O_5, indicating the existence of V^{5+} in the annealed film. Thus, its formula can be written as $V^{4+}_{0.875}V^{5+}_{0.125}O_{2.06}$. Moreover, according to the TGA data of the $VO_{2.06}$/RGO sample (Fig. 1b, curve ii), the weight loss of about 1.3% between 100 °C and 500 °C is attributed to the burning-out of RGO (weight loss) and the oxidation from VO_2 to V_2O_5 (weight gain). Thus, the mass content of carbon in the composite is estimated to be 9 wt%.

As shown in the SEM images of the cross section (Fig. 4a and b), the thickness of the film is around 20 μm and the structure is formed by the intertwining ribbons. This network is beneficial to achieve good contact between the ribbon and RGO, providing an easy electron pathway and a Li ion host. Based on the element mapping images (Fig. 4c) and energy-dispersive X-ray (EDX) analysis (Fig. 4d), it displays uniform distribution of C, V and O elements in the RGO covered vanadium oxide ribbon.

To study the Li-ion storage properties of this binder-free $VO_{2.06}$/RGO cathode film, a series of electrochemical measurements were carried out based on the half cell configuration. Fig. 5a shows the voltage profile of the free-standing film electrode at a current density of 70 mA g^{-1} (0.38 C) in a voltage range of 2.0–3.5 V. The mechanism for the charge/discharge of a crystalline VO_2 electrode can be described below [9,30]:

$$0.5Li^+ + 0.5e^- + VO_2 \rightleftarrows Li_{0.5}VO_2.$$

The reaction corresponds to a flat potential plateau at 2.5 V vs. Li^+/Li. However, the charge/discharge plateaus of this film electrode are not obvious (Fig. 5a), which should be due to the poor crystallinity of the film. According to above reaction, the theoretical capacity is 161 mAh g^{-1}. In our $VO_{2.06}$/RGO composite film, the insertion process gives an initial discharge capacity of 189 mAh g^{-1} and a subsequent charge capacity of 161 mAh g^{-1}. In contrast, the electrode without RGO only displays 112 mAh g^{-1} during first discharge process (Fig. 5b). The higher capacity for the $VO_{2.06}$/RGO film can be attributed to the faster kinetics of the lithium insertion and extraction. The intimate contact between the vanadium oxide ribbons and the graphene sheet provides both fast pathways for lithium ions and electrons. Some irreversible capacity loss is noticed in the first cycle, which is also observed for other simple metal-oxide intercalation compounds in literature [31–33]. It is possibly related to some structural rearrangement experienced by the material on the initial lithium uptake process. The electrode delivers a specific discharge capacity of 160 mAh g^{-1} in the second cycle, which remains at 156 mAh g^{-1} after 50 cycles, 148 mAh g^{-1} after 100 cycles and above 130 mAh g^{-1} after 200 cycles (Fig. 5b). This cycling performance is much better than the film without RGO prepared in this study, as well as the flexible free-standing VO_2 nanobelt film electrode (116 mAh g^{-1} at 50 mA g^{-1} during the first 50 cycles) [34] and other reported VO_2 cathodes [30,35]. The cycling responses of the free-standing $VO_{2.06}$/RGO film electrode at different C rates are evaluated and displayed in Fig. 5c. It shows an average discharge capacity of 141 mAh g^{-1} at a current density of 160 mA g^{-1} (0.87 C) and subsequently reduces to 118, 100, 87, 74 and 54 mAh g^{-1} at current densities of 320 (1.7 C), 480 (2.6 C), 640 (3.5 C), 800 (4.3 C) and 1120 mA g^{-1} (6.1 C), respectively. Electrochemical impedance spectra tests are carried out after the 20th cycle to explore the influence of the RGO (Fig. 5d). The $VO_{2.06}$/RGO film electrode shows a smaller radius of semi-circle in the Nyquist plots as compared to that of the free-standing vanadium oxide electrode without the modification of RGO, indicating the smaller charge-transfer resistance and the corresponding faster kinetics of

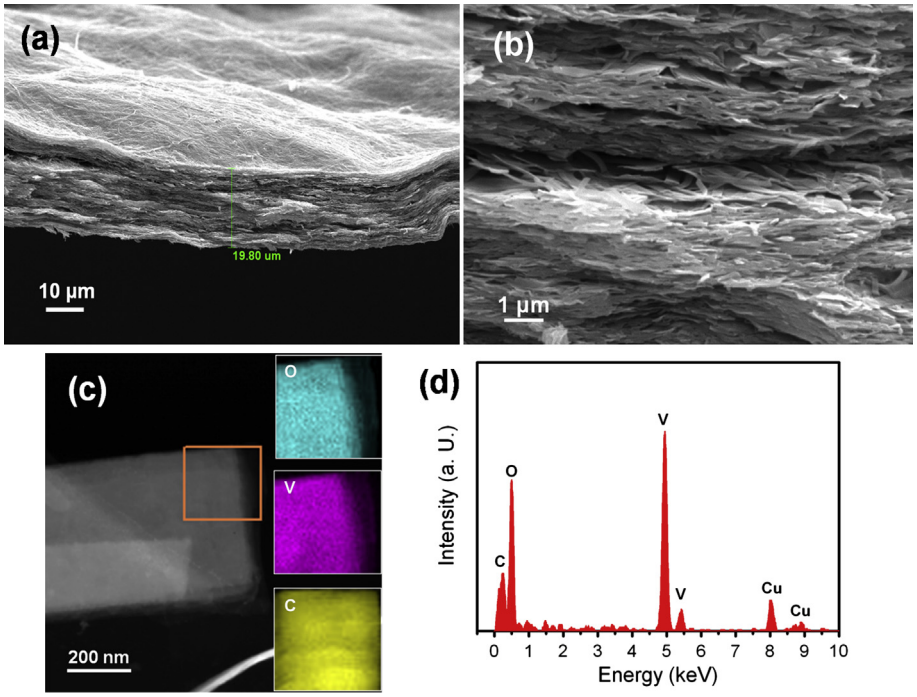

Fig. 4. (a, b) SEM images of cross section of VO_x/RGO film; (c) typical scanning transmission electron microscopy (STEM) image and corresponding elemental mapping images of oxygen, vanadium and carbon (inset of c) in the selected area; (d) energy-dispersive X-ray (EDX) spectrum, the peak of Cu is from the copper TEM grid.

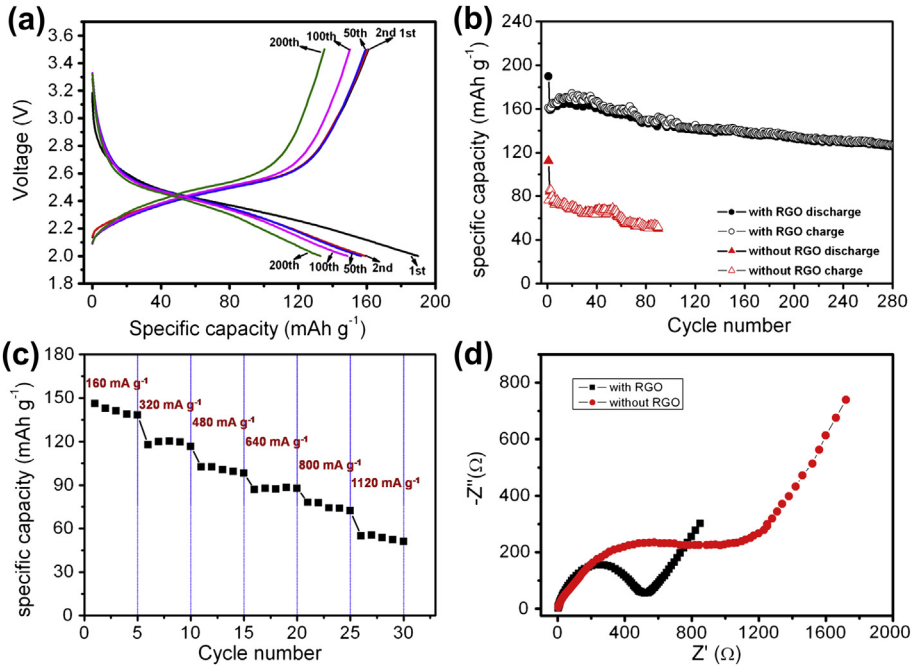

Fig. 5. (a) The voltage profile of VO_x/RGO film at a current density of 70 mA g^{-1}; (b) cycling performance of VO_x/RGO film and the VO_x film without RGO; (c) rate capability of VO_x/RGO; (d) electrochemical impedance spectra of these two film electrodes measured at the 20th fully discharged state.

the Faradic reaction. The good performance of this film electrode can be attributed to the following aspects: (1) the intertwining network of vanadium oxide ribbons with RGO provide efficient electron conduction pathways and short diffusion distances for Li ion intercalation/deintercalation; (2) the binder-free characteristic is beneficial to the electrical conductivity of electrode.

4. Conclusions

The hydrated vanadium pentoxide ribbons covered with reduced graphene oxide sheets are facilely synthesized by a hydrothermal process. A free-standing cathode film is prepared by using these ribbons and subsequently annealed in nitrogen. Different from the V_2O_5/RGO electrode reported in literature [18], the major phase of this binder-free film is VO_2. This cathode film delivers a high reversible specific capacity (160 mAh g^{-1}) and good cycling stability (133 mAh g^{-1} after 200 cycles). Such a composite film can be a potential binder-free cathode of rechargeable lithium batteries for desired energy storage applications.

Acknowledgments

This study was supported by National Science Foundation of China (grant nos. 20971117 and 10979049) and Education Department of Anhui Province (grant no. KJ2009A142). We are also grateful to the program of International Max Planck Research Schools and Solar Energy Operation Plan of Academia Sinica.

References

[1] S.Y. Chew, S.H. Ng, J.Z. Wang, P. Novak, F. Krumeich, S.L. Chou, J. Chen, H.K. Liu, Carbon 47 (2009) 2976.
[2] L.F. Cui, L.B. Hu, J.W. Choi, Y. Cui, ACS Nano 4 (2010) 3671.
[3] C.Y. Wang, D. Li, C.O. Too, G.G. Wallace, Chem. Mater. 21 (2009) 2604.
[4] A. Abouimrane, O.C. Compton, K. Amine, S.T. Nguyen, J. Phys. Chem. C 114 (2010) 12800.
[5] J.Z. Wang, C. Zhong, S.L. Chou, H.K. Liu, Electrochem. Commun. 12 (2010) 1467.
[6] C.M. Ban, Z.C. Wu, D.T. Gillaspie, L. Chen, Y.F. Yan, J.L. Blackburn, A.C. Dillon, Adv. Mater. 22 (2010) E145.
[7] C. Tsang, A. Manthiram, J. Electrochem. Soc. 144 (1997) 520.
[8] B. Zachauchristiansen, K. West, T. Jacobsen, Mater. Res. Bull. 20 (1985) 485.
[9] N.A. Chernova, M. Roppolo, A.C. Dillonb, M.S. Whittingham, J. Mater. Chem. 10 (2009) 2526.
[10] N. Ding, X.Y. Feng, S.H. Liu, J. Xu, X. Fang, I. Lieberwirth, C.H. Chen, Electrochem. Commun. 11 (2009) 538.
[11] S. Passerini, D.B. Le, W.H. Smyrl, M. Berrettoni, R. Tossici, R. Marassi, M. Giorgetti, Solid State Ion. 104 (1997) 195.
[12] M. Giorgetti, S. Passerini, W.H. Smyrl, S. Mukerjee, X.Q. Yang, J. McBreen, J. Electrochem. Soc. 146 (1999) 2387.
[13] M. Broussely, F. Perton, J. Labat, R.J. Staniewicz, A. Romero, J. Power Sources 43 (1993) 209.
[14] C. Delmas, H. Cognac-Auradou, J.M. Cocciantelli, M. Menetrier, J.P. Doumerc, Solid State Ion. 69 (1994) 257.
[15] C.K. Chan, H.L. Peng, R.D. Twesten, K. Jarausch, X.F. Zhang, Y. Cui, Nano Lett. 7 (2007) 490.
[16] C.K. Chan, H.L. Peng, G. Liu, K. McIlwrath, X.F. Zhang, R.A. Huggins, Y. Cui, Nat. Nanotechnol. 3 (2008) 31.
[17] H.Q. Li, T.Y. Zhai, P. He, Y.G. Wang, E. Hosono, H.S. Zhou, J. Mater. Chem. 21 (2011) 1780.
[18] X.H. Rui, J.X. Zhu, D.H. Sim, C. Xu, Y. Zeng, H.H. Hng, T.M. Lim, Q.Y. Yan, Nanoscale 3 (2011) 4752.
[19] G.D. Du, K.H. Seng, Z.P. Guo, J. Liu, W.X. Li, D.Z. Jia, C. Cook, Z.W. Liu, H.K. Liu, RSC Adv. 1 (2011) 690.
[20] H. Liu, W. Yang, Energy Environ. Sci. 4 (2011) 4000.
[21] H. Zhao, L. Pan, S. Xing, J. Luo, J. Xu, J. Power Sources 222 (2013) 21.
[22] W.S. Hummers, R.E. Offeman, J. Am. Chem. Soc. 80 (1958) 1339.
[23] Y.Y. Liang, J. Frisch, H.N. Arasi, X.L. Feng, J.P. Rabe, N. Koch, K. Mullen, Nanotechnology 20 (2009) 434007.
[24] H.K. Kim, S.M. Bak, K.B. Kim, Electrochem. Commun. 12 (2010) 1768.
[25] Z. Du, X. Yin, M. Zhang, Q. Hao, Y. Wang, T. Wang, Mater. Lett. 64 (2010) 2076.
[26] M. Giorgetti, S. Passerini, W.H. Smyrl, Inorg. Chem. 39 (2000) 1514.
[27] J.F. Liu, X. Wang, Q. Peng, Y.D. Li, Adv. Mater. 17 (2005) 764.
[28] E. Hryha, E. Rutqvist, L. Nyborg, Surf. Interface Anal. 44 (2012) 1022.
[29] G. Silversmit, D. Depla, Hi. Poelman, G.B. Marin, R.D. Gryse, J. Electron. Spectrosc. Relat. Phenom. 135 (2004) 167.
[30] X.H. Rui, D.H. Sim, C. Xu, W.L. Liu, H.T. Tan, K.M. Wong, H.H. Hng, T.M. Lim, Q.Y. Yan, RSC Adv. 2 (2012) 1174.
[31] G. Armstrong, J. Canales, A.R. Armstrong, P.G. Bruce, J. Power Sources 178 (2008) 723.
[32] A.R. Armstrong, G. Armstrong, J. Canales, R. Garcia, P.G. Bruce, Adv. Mater. 17 (2005) 862.
[33] P. Reale, S. Panero, B. Scrosati, J. Garche, M. Wohlfahrt-Mehrens, M. Wachtler, J. Electrochem. Soc. 151 (2004) A2138.
[34] J.J. Huang, X.F. Wang, J.F. Liu, X.M. Sun, L. Wang, X.M. He, Int. J. Electrochem. Sci. 6 (2011) 1709.
[35] C.V.S. Reddy, E.H. Walker, S.A. Wicker, Q.L. Williams, R.R. Kalluru, Curr. Appl. Phys. 9 (2009) 1195.